

Low-Complexity Adaptive Optics Aided Orbital Angular Momentum Based Wireless Communications

Huan Chang, Xiaoli Yin, Haipeng Yao, *Senior Member, IEEE*, Jingjing Wang, *Senior Member, IEEE*, Ran Gao, *Member, IEEE*, Jianping An, *Senior Member, IEEE*, and Lajos Hanzo, *Fellow, IEEE*

Abstract—Adaptive optics (AO) has the potential to mitigate the effect of atmospheric turbulence and improve the performance of orbital angular momentum (OAM)-based optical wireless communication (OAM-OWC) links. Here, we propose a single-intensity-measurement phase retrieval algorithm (SPRA)-based AO technique of compensating for the distortion of the OAM beam. The only parameter required by the SPRA wave-front sensor is the intensity of the probe beam in the Fourier domain, which substantially simplifies the AO system. We first derive an analytical expression to characterize the expansion of probe beam in OAM-OWC links and then determine the diameter constraints as the apriori information of the SPRA required for guaranteeing a certain compensation performance. The simulation results illustrate that the SPRA-AO approach can indeed correct a distorted OAM beam both in a single-channel scenario and in multiplexed OAM-OWC systems. The bit error rate can be improved by orders of magnitude with the aid of SPRA-AO compensation. Furthermore, we establish noise models of AO-based OAM-OWC systems and analyze the robustness of the SPRA-AO technique. In a nutshell, this paper provides new insights for the applications of AO and forms the theoretical basis of employing probe beams in OAM-OWC systems.

Index Terms—Optical wireless communications, orbital angular momentum, adaptive optics, phase retrieval algorithm.

I. INTRODUCTION

AS the demand for data increases, there is keen interest in increasing the transmission capacity in a range of fields [1], [2]. High-capacity optical wireless communication (OWC) is receiving increasing attention in various areas [3]–[5] because of the substantial demands for data transmission. Optical vortex beams carrying orbital angular momentum (OAM) characterized by a particular helical phase structure of $\exp(il\phi)$, have been introduced to meet the growing demand for large-capacity OWC [1], [6], [7] where the OAM state index l represents the number of 2π phase shifts across the beam and ϕ is the azimuthal angle. The OAM beams having a distinct l are orthogonal to each other, and the state index l is an infinite integer [8]. Therefore, the OAM beams are capable of substantially increasing the capacity of communication systems by either encoding information as OAM beam states or using OAM beams as information carriers for multiplexing [9]–[11].

The atmospheric turbulence (AT) effects, which are caused by random variations in temperature and convective motion induced by the random variations of the air's refractive index [12], constitute unavoidable impairments in OAM-aided OWC systems. In practical scenarios the atmospheric turbulence gives rise to phase distortion, which induces intermodal crosstalk among different states and degrades the performance of OAM-aided communication systems [13], [14]. Both experiments and simulations have verified that adaptive optics (AO) efficiently mitigates the distortion of OAM-OWC systems [15]. However, for OAM beams having helical phase fronts, one of the challenges is to directly detect the phase front using typical wave-front sensors due to the associated phase singularity [16]. To circumvent this, the phase retrieval algorithm (PRA)-based AO has gained increasing attention [17]. The Gerchberg-Saxton algorithm (GSA)-based phase correction method has been shown to efficiently mitigate the turbulent aberration of OAM beams both by simulations and experiments [18], [19]. Then, Fu *et al.* [20] used a probing Gaussian beam and the GSA for the pre-compensation of turbulence-infested OAM beams. In 2018, Yin *et al.* [21] proposed the hybrid-input-output-algorithm (HIOA) to compensate for the distortion of OAM beams in OAM-OWC systems.

Copyright (c) 2015 IEEE. Personal use of this material is permitted. However, permission to use this material for any other purposes must be obtained from the IEEE by sending a request to pubs-permissions@ieee.org.

This work was supported in part by the National Key R&D Program of China from Ministry of Science and Technology under Grant 2019YFA0706300, in part by the China Postdoctoral Science Foundation under Grant 2020M680385, 2020M680384, 2021M690411 and 2020TQ0054, in part by the National Natural Science Foundation of China under 62071062, 62022016, 61835002, 61727817, and in part by the Open Fund of IPOC (BUPT) under IPOC2020A007, IPOC2020A006. The work of H. Yao was supported by the Artificial Intelligence and Smart City Joint Laboratory (BUPT-TGSTII) (B2020001), Future Intelligent Networking and Intelligent Transportation Joint Laboratory (BUPTCTIC) (B2019007). The work of J. Wang was supported by the Young Elite Scientist Sponsorship Program by CAST under Grant 2020QNRC001. L. Hanzo would like to acknowledge the financial support of the Engineering and Physical Sciences Research Council projects EP/P034284/1 and EP/P003990/1 (COALESCE) as well as of the European Research Council's Advanced Fellow Grant QuantCom (Grant No. 789028). (*Corresponding author: Lajos Hanzo and Ran Gao.*)

H. Chang, R. Gao and J. An are with the School of Information and Electronics, Beijing Institute of Technology, Beijing 100081, China (email: 7520200099@bit.edu.cn; 6120190142@bit.edu.cn; an@bit.edu.cn).

X. Yin is with the School of Electronic Engineering, Beijing University of Posts and Telecommunications and also with the Beijing Key Laboratory of Space-Ground Interconnection and Convergence, Beijing University of Posts and Telecommunications, Beijing 100876, China (email: yinxl@bupt.edu.cn).

H. Yao is with the State Key Lab Networking & Switching Technol, Beijing University of Posts and Telecommunications, Beijing 100876, China (email: yaohaipeng@bupt.edu.cn).

J. Wang is with the Department of Electronic Engineering, Tsinghua University, Beijing, 100084, China (e-mail: chinaeephd@gmail.com).

L. Hanzo is with the School of Electronics and Computer Science, University of Southampton, Southampton, SO17 1BJ, UK (email: lh@ecs.soton.ac.uk).

TABLE I
COMPARISON OF THE PROPOSED SCHEME TO THE LITERATURE

| | Our paper | [13]-2020 | [4]-2019 | [5]-2018 | [20]-2017 | [19]-2016 | [13]-2015 | [18]-2012 | [33]-2010 |
|-----------------------------------|-----------|-----------|----------|----------|-----------|-----------|-----------|-----------|-----------|
| Optical Wireless Communication | ✓ | ✓ | ✓ | ✓ | ✓ | ✓ | ✓ | ✓ | |
| Orbital Angular Momentum | ✓ | | ✓ | ✓ | ✓ | ✓ | ✓ | ✓ | |
| Atmospheric Turbulence Simulation | ✓ | ✓ | ✓ | | ✓ | | | | |
| Adaptive Optics | ✓ | | ✓ | | ✓ | ✓ | ✓ | ✓ | |
| Shack-Hartmann wave-front | | | | | | | | | ✓ |
| Sensing technique | | | | | | | | | |
| Phase Retrieval Algorithm-based | ✓ | | | | ✓ | ✓ | | ✓ | |
| Wave-front sensing technique | | | | | | | | | |
| Probe Expansion | ✓ | | | | ✓ | | | | |
| Experimental AO analysis | | | | | | ✓ | ✓ | ✓ | |
| Simulation AO analysis | ✓ | | ✓ | | ✓ | | | ✓ | |
| Noise Model | ✓ | | | | | | | | ✓ |

The phase retrieval algorithm (PRA) has been conceived for reconstructing the phase from intensity information by exploiting any partial constraints, such as those observed in the object and Fourier domains. Explicitly, we have to infer the intensity of the probing beam in both the object and the Fourier domain as the input information of the algorithm to reconstruct the wave-front of the probe beam, which can be collectively termed as double-intensity measurements PRA (DPRA)-based AO (DPRA-AO) approaches [22], for both the HIOA and GSA [23]. These DPRA-AO systems require at least one beam splitter (BS) and two charge-coupled devices (CCDs). The BS halves the intensity of the probe beam, and the two CCDs constitute two detector-noise sources. On the other hand, compared to focused probe detection in the Fourier domain, optical detection in the object domain requires a wide field and imposes more detection noise.

We observe that in most cases of practical interest, the atmospheric phase is uniquely related to the Fourier intensity measurements [24]. Furthermore, AO in the communication links should ideally be miniaturized at a low cost [25], [26]. It is possible to recover the wave-front of the probe beam by solely relying on the intensity in the Fourier domain, provided that sufficient prior information is available about the probe beam [27]. Therefore, in this paper, we propose a low-complexity single-intensity-measurement PRA (SPRA)-based wave-front sensing technique for reconstructing the wave-front information of the probe beam relying on a low-complexity SPRA-based AO (SPRA-AO) system. The primary contributions of this paper are summarized as follows.

- We conceive a low-complexity and yet robust SPRA-AO technique which only has to detect a single Fourier intensity of the probe beam.
- An analytical expression is derived for characterizing the expansion of the OAM probe beam in an AO-based OAM-OWC system. Moreover, since there is a paucity of literature on this subject, the models of both the

background noise and of the CCD detector noise of DPRA-AO and SPRA-AO based OAM-OWC systems are established.

- Extensive simulations have been conducted for evaluating the performance of our proposed SPRA-AO, demonstrating that it improves the bit error rate (BER) by orders of magnitude. Furthermore, we demonstrate that SPRA-AO has better robustness than DPRA-AO in the face of both background noise and detector noise.

Our new contributions are boldly and explicitly contrasted to the literature at a glance in Table I.

The rest of this paper is organized as follows. Section II A describes the OAM-OWC system relying on the SPRA-AO technique. Section II B derives the analytical expression of the probe beam expansion in OAM-OWC links. Furthermore, the SPRA principle is introduced and its constraint setting is detailed in Section II C. Then, the models of both the background noise and of the detector noise of the PRA-AO approach are established in Section II D. Finally, Section III evaluates the compensation performance attained by the SPRA-AO technique, while Section IV concludes the paper.

II. CONCEPT AND PRINCIPLE

A. Schematic of an OAM-OWC system relying on the SPRA-AO technique

The schematic of our OAM-OWC system is shown in Fig. 1. At the transmitter, the OAM beam used for the desired signal and the probe beam are polarization-multiplexed by a polarizing beam splitter (PBS) and propagated collinearly through the atmospheric turbulence channel, where the probe beam is used for estimating the turbulence-induced distortions which can then be exploited for decontaminating the OAM beams [12]. The probe beam used for sampling the AT is expanded to a predetermined size as wide as that of the signal OAM beam relying on a beam expander [19]. During the propagation, the

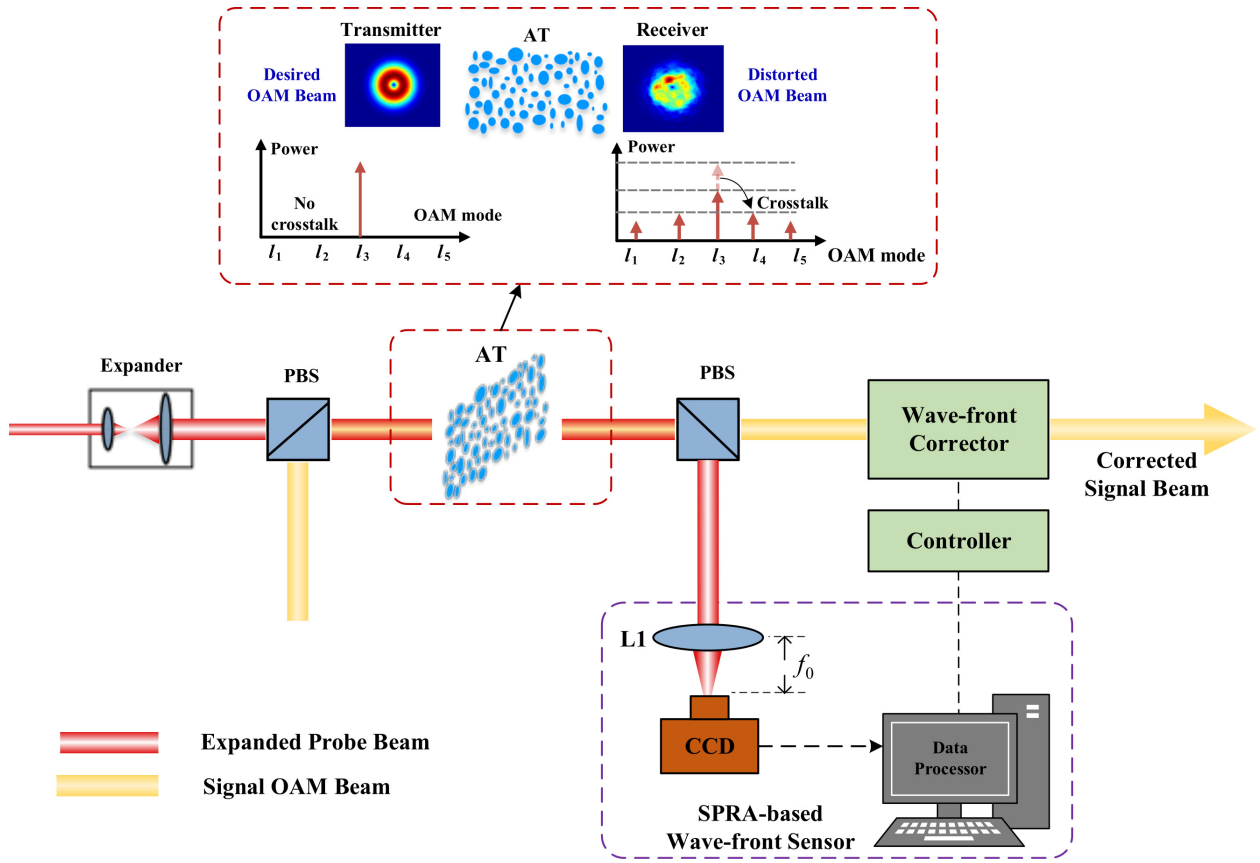


Fig. 1. Schematic of our OAM-OWC system equipped with an SPRA-AO module. (PBS: polarizing beam splitter, AT: atmospheric turbulence, L1: Fourier lens, f_0 : back focal length of L1.)

atmospheric turbulence impairs the propagation modes and spreads the emitted modes into adjacent modes. As shown in Fig. 1, the OAM beams having clear doughnut-like intensity distribution would become distorted [28], hence each particular OAM mode may become coupled with its neighbouring modes, and therefore the communication performance may be degraded [15]. The distorted multiplexed beams are then partitioned into the OAM signalling beam and the probe beam by using a PBS at the receiver. The probe beam is then entered into the AO module, which consists of the wave-front sensor, wave-front controller and wave-front corrector. The wave-front sensor surrounded by a dashed line in Fig. 1 is composed of the Fourier lens L1, a CCD camera and a data processor. The Fourier lens L1 of Fig. 1 is used here to focus the beam and to estimate the spatial spectral distribution of the probe beam. The CCD camera of Fig. 1 in the focal plane of L1 is used for capturing the Fourier intensity pattern of the probe beam. Then, the data processor retrieves the phase of the probe beam from the focal plane intensity information with the aid of the SPRA and estimates the phase-change induced by turbulence. Finally, the estimated phase-correction signal is forwarded by the controller to the wave-front corrector of Fig. 1 for decontaminating the signal beam.

The Laguerre-Gaussian (LG) beam is a simple and widely used vortex beam, which can be characterized by a pair of indices, i.e. the azimuthal index l and the radial index p [29]. Hence, we consider it as an example in our analysis. The LG

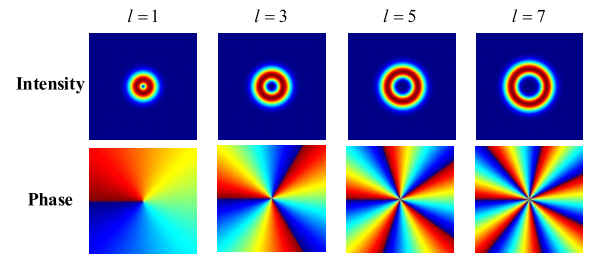


Fig. 2. Intensity and phase distributions of LG beams with different azimuthal state indexes.

modes having different l values or p values are orthogonal to each other. In the classical domain, mode multiplexing (i.e., each mode carries an independent data stream) and data encoding (i.e., each pulse occupies a given LG mode state) using different l or p values have the potential of substantially increasing the capacity of communication systems [30]. The intensity and phase distributions of LG beams associated with different azimuthal state indices are shown in Fig. 2, where the doughnut-shaped intensity profiles are clearly visible because of the phase singularity at the beam center. The definition of an LG mode [30] that gives the intensity distribution for the lowest-order radial LG mode $p = 0$ can be formulated as:

$$I(r, \phi, z) = \frac{2}{\omega^2(z)\pi |l|!} \left[\frac{r\sqrt{2}}{\omega(z)} \right]^{2|l|} \exp \left[\frac{-2r^2}{\omega^2(z)} \right], \quad (1)$$

which is normalized as $\int_0^\infty \int_0^{2\pi} I(r, \phi, z) r d\phi dr = 1$. In (1), r is the radial cylindrical coordinate, ϕ represents the azimuthal angle and l is the azimuthal state index. Moreover, $\omega(z)$ denotes the beam radius at the propagation distance z , which can be expressed as

$$\omega(z) = \sqrt{\omega_0^2 + (z/z_R)^2}, \quad (2)$$

where λ is the optical wavelength, while $z_R = \pi\omega_0^2/\lambda$ is the Rayleigh range and ω_0 represents the $1/e$ radius of the Gaussian term of the LG beam, which is also termed as the beam waist [31]. In the AO-based OAM-OWC system of Fig. 1 we utilize the OAM beam as the probe beam, because the OAM beam associated with hollow intensity and used as a probe beam outperforms the Gaussian probe beam in AO-based OAM systems [22].

B. The expansion scheme of the probe beam in OAM-OWC systems

In an AO-based OAM-OWC system, the phase-change imposed by atmospheric turbulence is estimated by the probe beam and then used for the decontamination of the signal beam. For achieving more accurate phase compensation, the expanded probe beam should remain as wide as the signal beam during their collinear propagation in order to satisfy the assumption that the OAM signalling beam and probe beam undergo similar wave-front aberrations because of turbulence [32]. However, if the probe beam is much wider than the signal beam, the probe beam will experience more severe turbulence-induced distortion than the signal beam. It has been demonstrated that the degree of wave-front aberration similarity between the signal and probe beam depends to some extent on the intensity distribution similarity of these two beams. In other words, the AO compensation performance is also affected by the intensity distribution similarity of the signal and the expanded probe beam. Fig. 3 shows the intensity distributions of the OAM signalling beam and expanded probe beam during their propagation. Therefore, in this section, we conceive a beneficial scheme for ensuring that the intensity distributions of the two beams remain similar.

For convenience, the notations used in the following derivation are summarized at a glance in Table II. We define the intensity correlation coefficient [33] between the signal beam and the expanded probe beam as follows:

$$C = \frac{\int_0^\infty \int_0^{2\pi} I_p(r, \phi, z) \cdot I_s(r, \phi, z) r d\phi dr}{\sqrt{\int_0^\infty \int_0^{2\pi} I_p^2(r, \phi, z) r d\phi dr \cdot \int_0^\infty \int_0^{2\pi} I_s^2(r, \phi, z) r d\phi dr}}, \quad (3)$$

where $I_p(r, \phi, z)$ and $I_s(r, \phi, z)$ are the intensities of the probe beam and signal beam, respectively. Combined with (1) and (3), C can be reformulated as

TABLE II

THE EXPLANATION OF NOTATIONS IN THE FOLLOWING DERIVATION.

| Notation | Declarations | Notation | Declarations |
|----------------|------------------------------------|----------------|-------------------------------------|
| I_p | The intensity of the probe beam | I_s | The intensity of the signal beam |
| l_p | The state number of the probe beam | l_s | The state number of the signal beam |
| $\omega_p(z)$ | The beam radius of the probe beam | $\omega_s(z)$ | The beam radius of the signal beam |
| ω_{0_p} | The beam waist of the probe beam | ω_{0_s} | The beam waist of the signal beam |

$$C = \left(\frac{1}{\omega_s(z)} \right)^{1+2|l_s|} \left(\frac{1}{\omega_s^2(z)} + \frac{1}{\omega_p^2(z)} \right)^{-1-|l_s|-|l_p|} \cdot \left(\frac{1}{\omega_p(z)} \right)^{1+2|l_p|} \cdot 2^{1+|l_s|+|l_p|} \cdot \frac{\Gamma(1+|l_s|+|l_p|)}{\sqrt{\Gamma(1+2|l_s|) \cdot \Gamma(1+2|l_p|)}}, \quad (4)$$

where $\Gamma(\cdot)$ represents the classical gamma function.

We can derive the optimal beam waist ω_{0_p} of the probe beam for maximizing C by solving the following equation

$$\frac{\partial C}{\partial \omega_{0_p}} = \frac{\partial C}{\partial \omega_p} \cdot \frac{\partial \omega_p}{\partial \omega_{0_p}} = 0. \quad (5)$$

Upon combining (2) and (5), and solving (5), we can determine the relationship between $\omega_p(z)$ and $\omega_s(z)$

$$\omega_p(z) = \sqrt{\frac{2|l_s|+1}{2|l_p|+1}} \cdot \omega_s(z). \quad (6)$$

The mathematical expression of the probe beam broadening in an OAM-OWC link is shown in (6). When the beam radii of the probe and signal beam satisfy the relationship shown in (6), the correlation coefficient C is maximized, as is the intensity distribution similarity of the two beams.

Note that the optimal beam waist of the probe beam is calculated by (2) and (6) based on the longest propagation distance. The above derivation describes a single OAM channel associated with the transmission state index l_s . By contrast, for multiple links, $|l_s|$ represents the maximum absolute value of the state index in the transmitted OAM beams [22].

C. Single-intensity-measurement based phase retrieval algorithm

In this section, we describe an SPRA that estimates the wave-front of an OAM beam based on its Fourier intensity and on the knowledge of the object constraints. The flow-chart of the SPRA is shown in Fig. 4.

Let us denote the optical field of the received probe beam in the object domain as $f(x, y)$ and in the Fourier domain as $F(u, v)$, where (x, y) are the associated spatial coordinates and (u, v) are the spatial frequency coordinates. The object domain represents here the distorted probe beam $f(x, y)$ of

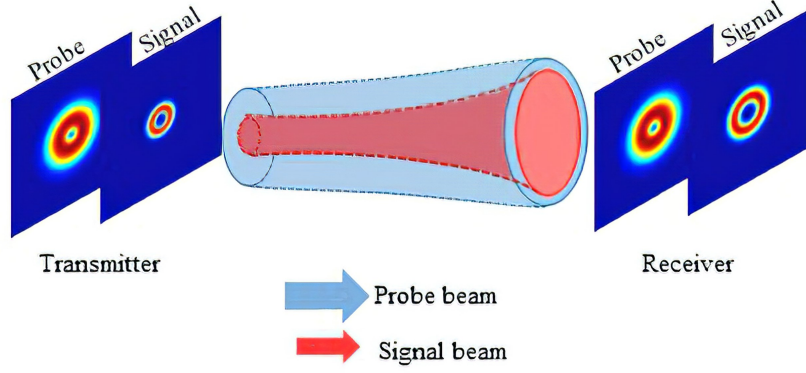


Fig. 3. Stylized propagation of both the OAM signalling beam and expanded probe beam.

the OAM-OWC system, which corresponds to the optical field distribution in the front focal plane of L1 in Fig. 1. Furthermore, $|F(u, v)|$ is the real-valued modulus obtained by taking the square root of the Fourier intensity of the object, which is measured by the CCD of Fig. 1.

Appropriate initialization assists in prompt and accurate convergence. We set the initial estimated object of the SPRA to $g_0(x, y) = \mathcal{F}^{-1}\{|F(u, v)| \cdot e^{j\theta_0(u, v)}\}$, where θ_0 is set to the phase distribution of the no-turbulence probe beam in the Fourier domain. As shown in Fig. 4, the SPRA consists of the following four steps at the k -th iteration [24]:

- (1) From g_k to G_k : Fourier transform g_k ;
- (2) From G_k to G'_k : Replace the modulus of the resultant Fourier transform G_k with the aid of the measured Fourier modulus $|F(u, v)|$ in order to form an estimate of the Fourier transform G'_k ;
- (3) From G'_k to g'_k : Inverse Fourier transform the estimate of the Fourier transform G'_k in order to form an estimate of the object g'_k ;
- (4) From g'_k to g_{k+1} : Calculate the input of the next iteration g_{k+1} that satisfies the object constraints [23]. The fourth step is designed by referring to the negative feedback, which can be expressed as

$$g_{k+1}(x, y) = \begin{cases} g'_k(x, y), & (x, y) \in \gamma, \\ g_k(x, y) - \beta g'_k(x, y), & (x, y) \notin \gamma, \end{cases} \quad (7)$$

where γ represents the object constraints and β is a constant feedback parameter having typical values between 0.5 and 1.

The algorithm terminates when the iterations satisfy the termination criterion or reach a given number.

In the proposed SPRA the only known information is the modulus in the Fourier domain $|F(u, v)|$, hence we need sufficient prior information about the object in order to estimate its phase accurately [34]. The OAM beam has the unique characteristic that the beam width is related both to the state index and to the beam waist [31]. In order to achieve accurate compensation, we rely on the diameter constraints as the prior information in the SPRA.

For considering the intensity distribution of the OAM beam, we introduce the diameter constraints as partial constraints of

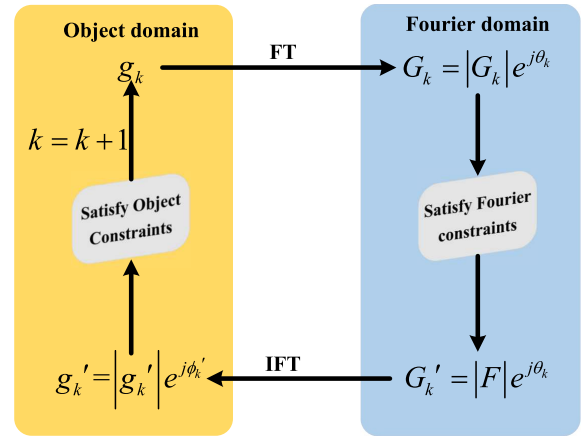


Fig. 4. The flow-chart of the SPRA. (FT: Fourier transformation; IFT: inverse Fourier transformation.)

the object quantified by the centrosymmetric circular region γ , which contains more than 99% of the transmitted intensity of the probe beam. The radius of the circular region can be expressed as

$$R_C = 2\omega_p(z)\sqrt{|l_p| + 1}, \quad (8)$$

where $\omega_p(z)$ and l_p represent the beam radius and state index of the probe beam, respectively [24]. An example of the object constraint is given in Fig. 5 from the perspectives of the intensity distribution and the line intensity profile¹. As shown in Fig. 5, for $(x, y) \in \gamma$ of the distorted probe beam, the next estimated object g_{k+1} is equal to g'_k . We assume that the intensity of the probe beam in the absence of turbulence in $(x, y) \notin \gamma$ is zero. Therefore, for $(x, y) \notin \gamma$, the SPRA provides negative feedback from the most recently estimated object g_k to drive the next estimated object g_{k+1} towards zero, as shown in (7) [22].

D. Robustness analysis of PRA-AO techniques

Sensing light intensity is fundamental to any wave-front sensor technique [27]. As mentioned above, both the DPRA-

¹Line intensity profile is defined as the two-dimensional intensity distribution along the horizontal radial vortex centers of the OAM beam.

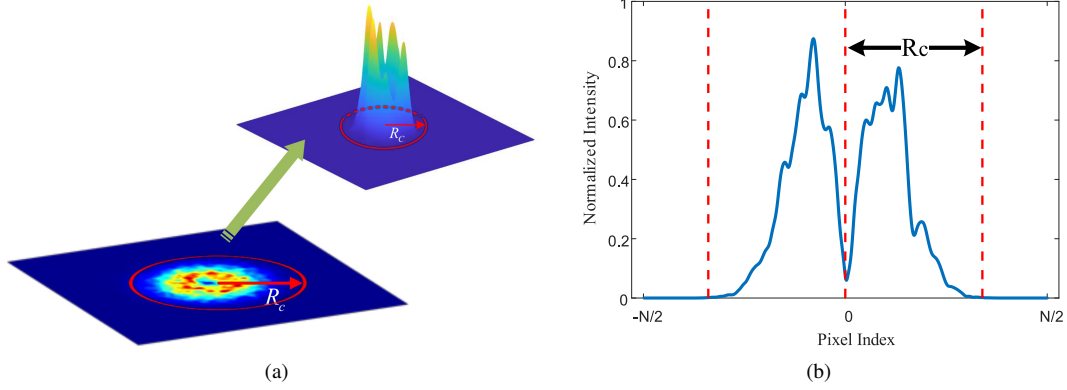


Fig. 5. (a) The object constraints and the intensity distribution of the broadened probe beam. (b) Diagram of the constraints and the line intensity profile along the center of the probe beam. (N : the number of grid points.)

TABLE III
THE EXPLANATIONS OF THE NOISE TYPES USED IN THE NOISE MODEL

| Noise type | Notation | Noise model |
|------------------|-----------|------------------------------|
| Background noise | N_0 | Complex Gaussian white noise |
| Detector noise | N_i | Shot noise and readout noise |
| Shot noise | N_{s_i} | Poisson noise |
| Readout noise | N_{r_i} | Gaussian white noise |

AO and SPRA-AO estimate the phase impairment from the measured intensity information, and it is vitally important to analyze the detector-noise resistance of PRAs. At the time of writing there is a paucity of literature on the robustness of the AO approach in OAM-OWC links. We commence our evaluation of the robustness of SPRA-AO techniques by establishing the noise model of the SPRA-AO and DPRA-AO. The principle of GSA-AO has been detailed in [21], while the schematic of the DPRA-AO and SPRA-AO techniques and their noise models are shown in Fig. 6(a) and Fig. 6(b), respectively.

The noise components contaminating the detectors are assumed to be independently and identically distributed and their features are shown at a glance in Table III. The background noise, denoted as N_0 , is modeled by a complex Gaussian white noise process of mean 0 and variance σ_0^2 [35], [36]. As for the CCD detector noise, we consider the situation in which the detector noise consists of a combination of shot noise and readout noise. The shot noise is mainly a combination of photon noise and dark noise, both exhibiting a Poisson distribution, since they are based on the random arrival of photons at the CCD of Fig. 6 [37]. The readout noise is imposed on the signal during the process of measuring the signal and it is also assumed to be Gaussian white noise of mean 0 and variance σ_1^2 [38]. The detector noise N_j is given by [39]

$$N_j = N_{s_j} + N_{r_j} \quad i = (1, 2, 3), \quad (9)$$

where j represents the CCD index of Fig. 6. Note that there is no extra parameter associated with the Poisson noise, but the noise magnitude depends on the intensity of the signal entering the CCD [40].

At the receiver, the contaminated probe beam is denoted as $u_r(r, \phi, z)$, which contains the additive background noise N_0 perturbing the multiplexed beam. For the DPRA-AO technique associated with the noise model of Fig. 6(a), the two inputs of the DPRA can be expressed as [21]

$$|f(x, y)| = \sqrt{I_{CCD1}} = \sqrt{\frac{|u_r(r, \phi, z)|^2}{2} + N_1}, \quad (10)$$

$$|F(u, v)| = \sqrt{I_{CCD2}} = \sqrt{\left| \mathcal{F} \left[\frac{u_r(r, \phi, z)}{\sqrt{2}} \right] \right|^2 + N_2}. \quad (11)$$

For the SPRA-AO technique having the noise model of Fig. 6(b), one of the SPRA inputs is expressed as

$$|F_s(u, v)| = \sqrt{I_{CCD3}} = \sqrt{\left| \mathcal{F} [u_r(r, \phi, z)] \right|^2 + N_3}, \quad (12)$$

where I_{CCD3} represents the intensity captured by the CCD₃ of Fig. 6(b) and N_3 is the additive detector noise contaminating the magnitude of the probe beam in the Fourier domain for the SPRA.

III. SIMULATIONS AND DISCUSSIONS

In the following, we simulate the propagation of the OAM beam in AT with random phase screens based on Kolmogorov's turbulence theory along the propagation path. The random process of turbulence is typically characterized in statistical theory, because the complexity of the atmosphere does not lend itself to prediction and numerical analysis. Kolmogorov's turbulence theory describes the average effects of total beam wander, beam spreading, and scintillation [41]. In our study, the propagation of the OAM beams through a locally homogeneous and isotropic turbulent medium, which exhibits modified Von-Karman atmospheric phase characteristics [42], is modeled relying on the simulation tool MATLAB. The structure constant of the refractive index C_n^2 is varied in the range of $1 \times 10^{-16} \sim 1 \times 10^{-14} \text{m}^{-2/3}$. As for the simulation parameters, the number of grid points per side is 756. The wavelength λ is set to 532nm. The number of random phase screens is 11 along the propagation path. Furthermore,

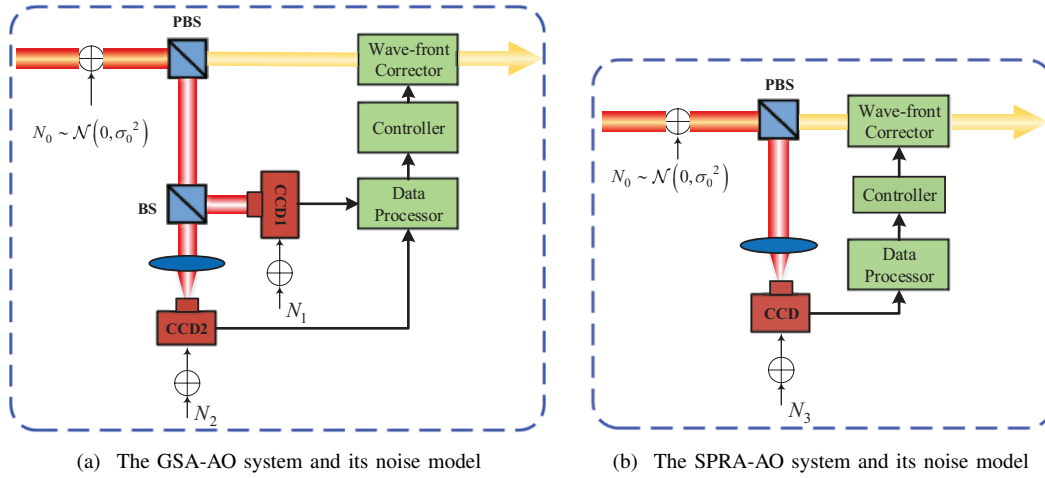


Fig. 6. Schematic of the AO system and its noise model. (BS: beam splitter (50:50).)

the outer and inner scale of turbulence are 50m and 0.01m, respectively. The receiver aperture size is set to 0.3m and the β factor of the SPRA is set to 0.7 [31]. For a given propagation distance, we set the waist of the signal beam to $\omega_{0-s} = \sqrt{\lambda z / \pi}$ at the transmitter [43]. As for the parameters of the probe beam, the probe beam is an OAM beam associated with $l_p = 1$ and the waist of the expanded probe beam follows (6). As an example, for $z = 400\text{m}$ and $l_s = 3$, the waist of the signal beam ω_{0-s} is 0.0082m and the waist of probe beam ω_{0-p} can be calculated as 0.017m.

A. Compensation performance analysis of the SPRA-AO technique

The OAM spectrum is calculated by relying on the so-called modal decomposition method to characterize the ratio of the power retained by the original transmit state and of the power spread into the adjacent channels. The power associated with the OAM spectrum characterizes the specific proportion of each state [44]. We define the mode purity as the relative power of the desired transmit state in the OAM spectrum, and define the crosstalk as the relative power of the undesired state. The values of mode purity and crosstalk are between 0 and 1, where high mode purity and low crosstalk correspond to a better quality of the OAM beam. Moreover, we define the squared error (SE) function for quantifying the compensation performance, which can be expressed as

$$\text{SE} = \sum_i |p_w(i) - p_0(i)|^2, \quad (13)$$

where the variable i represents the state index of the OAM beam; $p_w(i)$ is the relative power of the OAM state index i of the OAM beam with/without SPRA-AO compensation; and $p_0(i)$ is the relative power of the OAM state index i of the desired OAM beam in the absence of turbulence. A smaller SE value corresponds to a better correction performance.

We consider the OAM states $l = 3$ and $l = \{-1, +2\}$ as examples of single-channel and multiplexed-channel communication, respectively, for characterizing the compensation performance of the SPRA-AO technique. Fig. 7 shows the

spectrum of the OAM signal beams both with and without SPRA-AO compensation under different turbulence strengths. The SE values are labeled in Fig. 7(a) - 7(f), where SE_0 corresponds to the SE values before compensation, while SE_1 corresponds to the values after SPRA-AO compensation. The SPRA-AO technique has substantial advantages in terms of accuracy by mitigating the impairments of both single-channel and multiplexed OAM-OWC systems. After SPRA-AO compensation, the relative power of the desired state increases, while the crosstalk between adjacent states is mitigated, hence the SE values are significantly reduced. Explicitly, the mode purity is improved from 0.52 to 0.74 after compensation, as shown in Fig. 7(b). In Fig. 7(c), the crosstalk of $l = 3$ imposed on the adjacent mode $l = 2$ is significantly reduced from 0.37 to 0.13 after compensation. Furthermore, the squared error is reduced from 0.11 to 0.04 after compensation, as seen in Fig. 7(e).

To illustrate the improvement of system's power penalty, the bit error rate (BER) both with and without SPRA-AO compensation is calculated based on [28], when an OAM beam associated with $l = 3$ is transmitted under the atmospheric structure constants of $C_n^2 = 1 \times 10^{-15} \text{m}^{-2/3}$ and $C_n^2 = 1 \times 10^{-14} \text{m}^{-2/3}$. The traditional GSA-AO scheme is used for benchmarking the BER improvement of the SPRA-AO and DPRA-AO techniques. During the BER calculations, we assume that on-off keying or binary pulse position modulation is used [30]. Fig. 8 presents the BER curves as a function of the optical signal-to-noise ratio (OSNR), when an OAM beam with $l = 3$ is transmitted [11]. Fig. 8(a) and 8(b) show that after SPRA-AO compensation, the BER performance improves as a benefit of the corrected OAM beam, and the BER falls below the forward error correction (FEC) limit of 3.8×10^{-3} . Furthermore, the BER is considerably reduced from 0.275 to 1.2×10^{-4} and 3.1×10^{-4} relying on SPRA-AO and GSA-AO compensation, when the OSNR is set to 17dB, as shown in Fig. 8(b). It can be concluded from Fig. 8(a) and (b) that our low-complexity SPRA-AO achieves a similar compensation performance to that of GSA-AO.

The convergence performance is a critical performance

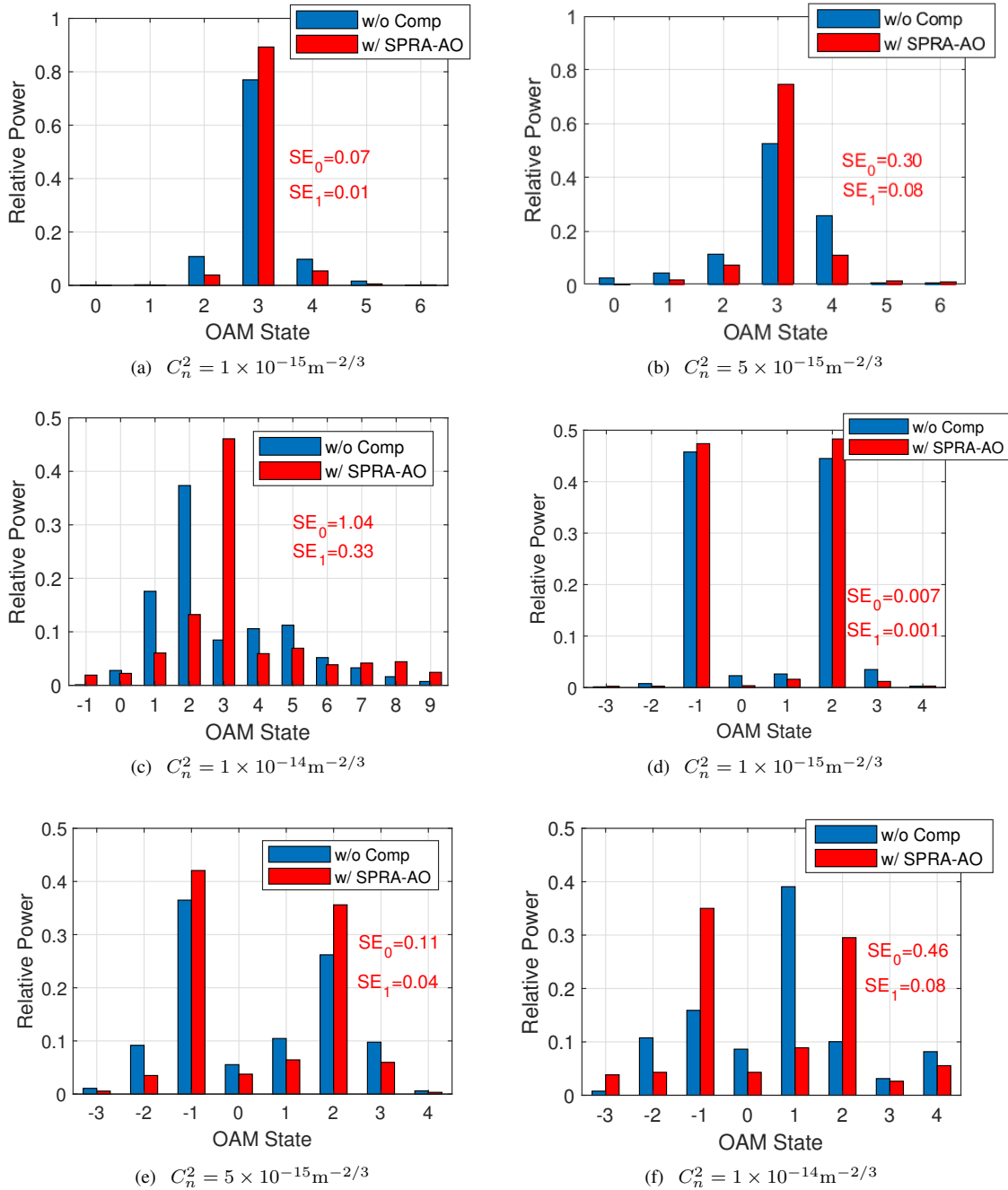


Fig. 7. OAM spectrum of the OAM beam with or without SPRA-AO compensation. (a)-(c) In the case of a single-OAM link for $l = 3$. (d)-(f) In the case of a multiplexed-channel link for $l = \{-1, +2\}$. The propagation distance is 400 m.

criterion of the algorithm. The traditional GSA-AO scheme is used for benchmarking the convergence performance of the SPRA and GSA. The OAM spectrum of the signal beam using $l = 3$ before and after SPRA-AO and GSA-AO compensation is shown in Fig. 9(a), while the corresponding convergence curve is shown in Fig. 9(b). It can be concluded from Fig. 9(a) and 9(b) that SPRA-AO and GSA-AO can achieve a similar compensation performance and then the SPRA exhibits better convergence speed than the GSA.

B. Discussion of the probe beam expansion

Recall from Section II B that for accurate phase-compensation the expanded probe beam has to remain wider than the signal beam during their collinear propagation. Hence, to reflect the benefits of the probe beam expansion, we now carry out a detailed comparative analysis of three different expansion schemes. The beam waist of the probe beam associated with the different expansion schemes is listed in Table IV, where ω_{0_s} is the beam waist of the signal beam and ω_{0_p} is that of the expanded probe beam calculated according to (8). As shown in Table IV, the beam waist of the probe is

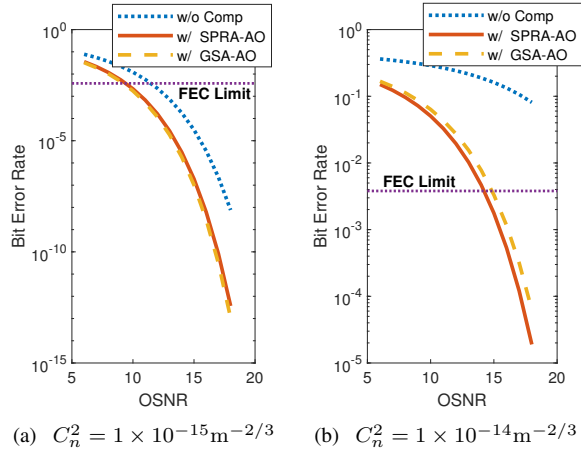


Fig. 8. BER as a function of the OSNR when an OAM beam using $l = 3$ is transmitted both with and without SPRA and GSA-AO compensation for different atmospheric structure constant. The propagation distance is 400 m.

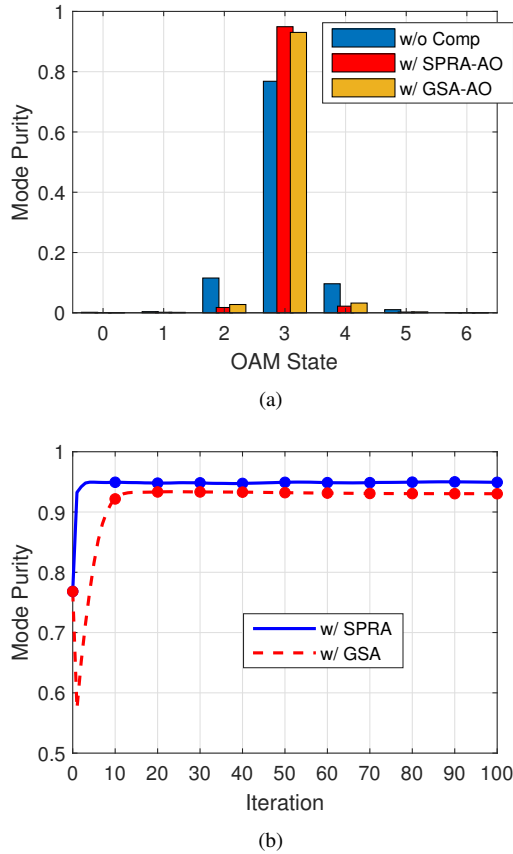


Fig. 9. (a) The OAM spectrum of the signal beam associated with $l = 3$ both before and after SPRA-AO and GSA-AO compensation. (b) Mode purity as a function of the number of iterations for the SPRA and GSA. ($C_n^2 = 2 \times 10^{-15} \text{m}^{-2/3}$)

TABLE IV
THE BEAM WAIST OF THE PROBE BEAM WITH DIFFERENT EXPANSION SCHEME

| Expansion scheme | Without expansion | Expansion 1 | Expansion 2 |
|--------------------------|-------------------|----------------|-----------------|
| Beam waist of probe beam | ω_{0_s} | ω_{0_p} | $2\omega_{0_p}$ |

TABLE V
THE DETAILED PARAMETERS OF THE DIFFERENT EXPANSION SCHEMES

| Parameter Type | Value |
|--|---------|
| State index of signal beam | 3 |
| State index of probe beam | 1 |
| Beam waist of signal beam | 0.0082m |
| Beam waist of probe beam without expansion | 0.0082m |
| Beam waist of probe beam with Expansion 1 | 0.0173m |
| Beam waist of probe beam with Expansion 2 | 0.0346m |

equal to that of the signal if there is no probe expansion. In this context, Expansion 1 represents the scheme we proposed in Section II B, while Expansion 2 represents an oversized probe beam. The detailed parameters with different expansion scheme are shown in Table V.

The curves of the mode purity and the OAM state index recorded both before and after compensation are shown in Fig. 10. The curve marked by stars represents the mode purity after SPRA-AO compensation using Expansion 1, while the curves marked by triangles and squares represent the mode purity after compensation without probe expansion and with Expansion 2, respectively. The results show that the SPRA-AO relying on the proposed expansion scheme substantially improves the mode purity of OAM beams having different state indices and reduces the distortion of the OAM beam. Furthermore, Fig. 10 shows that the mode purity recorded either after compensation without expansion or by using an inappropriate oversized expansion (Expansion 2) is even lower than that without compensation, confirming that beam expansion is necessary in a high-performance AO system.

This phenomenon of Fig. 10 can be explained as follows by relying on a signal beam associated with $l = 7$ as an example. Fig. 11 shows the line intensity profiles² along the vortex centers of the signal beam and probe beam both with and without expansion. Compared to the probe beam without expansion or to that with oversized expansion, the probe beam using the proposed expansion has a more similar cross section of the intensity distribution to that of the signal beam and undergoes more similar wave-front aberration, when propagating collinearly with the signal beam through atmospheric turbulence.

The relationship between the propagation distance and mode purity of the signal beam of $l = 7$ before and after compensation is shown in Fig. 12. Each value of mode purity represents an average of 100 realizations. The curve marked with stars in Fig. 12 shows that the SPRA-AO technique compensates the distorted OAM beam quite effectively within 800 m. Fig.

²How these were generated was discussed in a footnote in Section II C.

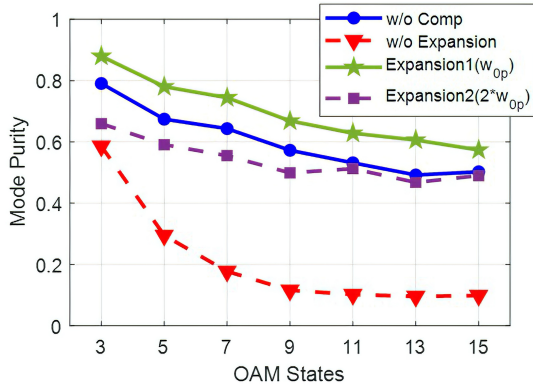


Fig. 10. Mode purity as a function of the transmission state index of signal beams before/after the SPRA-AO operating both with and without probe beam expansion. ($C_n^2 = 2 \times 10^{-15} \text{m}^{-2/3}$, $z = 400\text{m}$.)

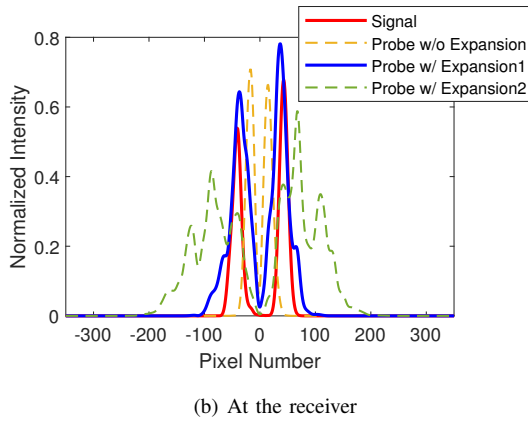
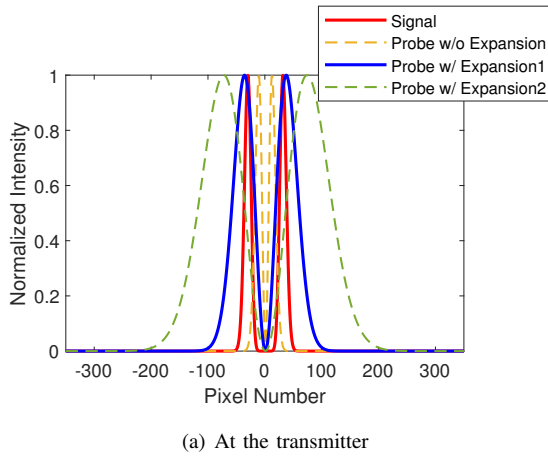


Fig. 11. Line intensity profiles along the vortex centers of the signal beam with $l=7$ and the probe beam with and without expansion. ($C_n^2 = 2 \times 10^{-15} \text{m}^{-2/3}$, $z = 400\text{m}$.)

12 also indicates the importance of using the most appropriate expansion of the probe beam in an AO system.

C. Robustness analysis of the SPRA-AO technique

Having verified the efficiency of the SPRA-AO technique and the benefits of probe expansion, we now further analyze

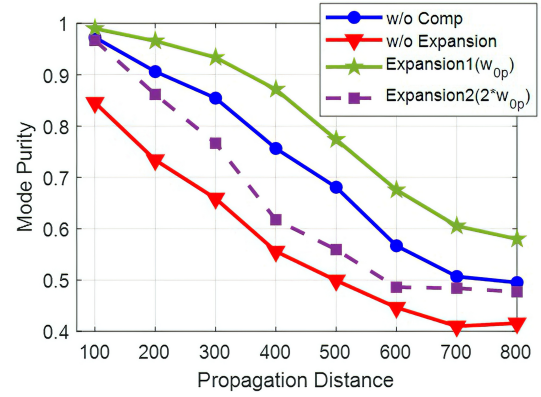


Fig. 12. Mode purity of the signal beam versus the propagation distance with/without SPRA-AO compensation. ($C_n^2 = 2 \times 10^{-15} \text{m}^{-2/3}$.)

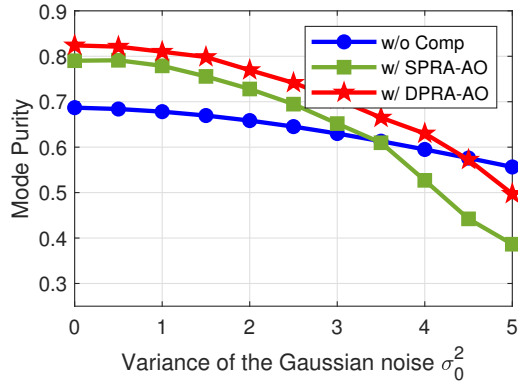
the robustness of the SPRA-AO against both the background noise and the CCD detector noise.

We first qualify how the background noise affects the compensation performance of the PRA-AO systems. Fig. 13(a) shows the mode purity as a function of σ_0^2 using the SPRA-AO and DPRA-AO techniques when only the background noise N_0 exists. We run the tests 100 times under different σ_0^2 values and take the average of the mode purity results. Fig. 13(a) shows that despite AO compensation, the mode purity is reduced upon increasing σ_0^2 , which means that the background noise degrades the AO compensation performance regardless of whether the SPRA-AO or the DPRA-AO technique is used. In Fig. 13(a), the mode purity equals to 0.65, 0.72 and 0.77 before compensation as well as after SPRA-AO and DPRA-AO compensation, respectively, when $\sigma_0^2 = 2$. This trend is indeed expected because the intensities in both the object and the Fourier domain are exploited as prior information by the DPRA, while the SPRA uses only the intensity in the Fourier domain as its measured input. It can be concluded that the SPRA-based AO technique exhibits eroded compensation performance with less prior information in exchange for its simplicity.

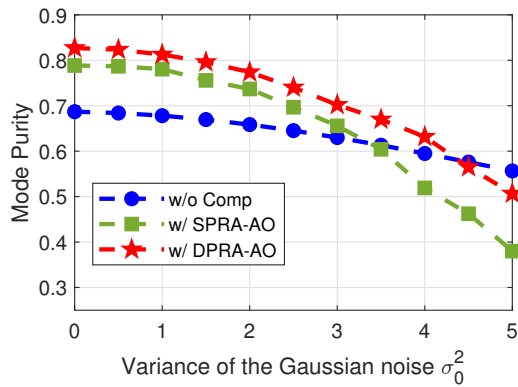
The curves of the mode purity vs σ_0^2 are shown in Fig. 13(b), when both the background noise and the shot noise of the detector exist. Observe that the mode purity seen in Fig. 13(a) and Fig. 13(b) both with and without shot noise are similar. Therefore, the shot noise is not the dominant factor that affects the compensation performance. It can be concluded that both SPRA-AO and DPRA-AO are robust against shot noise.

Let us now introduce both background noise and detector noise - including shot noise and readout noise - into the AO module. The mode purity vs the readout Gaussian noise variance σ_1^2 is shown in Fig. 14, where we observe that upon increasing σ_1^2 , the mode purity of SPRA-AO compensation is seen to be more stable than that having DPRA-AO compensation. We conclude that SPRA-AO exhibits unique robustness than DPRA-AO in AO-based OAM-OWC systems.

This phenomenon can be explained as follows. Recall from Fig. 6 that in the DPRA-AO system, the contaminated probe beam is split by a BS into two copies for detecting the intensities in the object and Fourier domain. The split input



(a) Only background noise exists



(b) Both the background noise and the shot noise of the CCD detector exist

Fig. 13. Mode purity versus the background noise variance σ_0^2 for the SPRA and DPRA-AO techniques, when an OAM beam associated with $l = 3$ is transmitted. ($C_n^2 = 3 \times 10^{-15} \text{m}^{-2/3}$, $z = 400\text{m}$.)

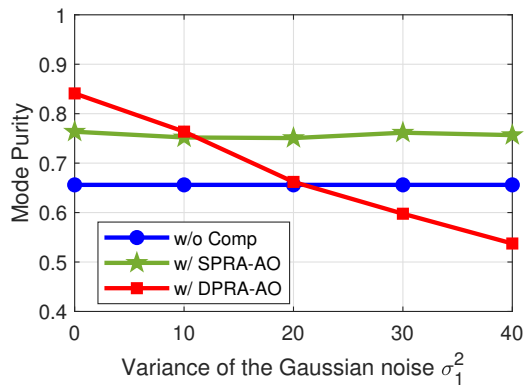


Fig. 14. Mode purity as a function of the Gaussian noise variance when an OAM beam with $l = 3$ is transmitted. ($C_n^2 = 3 \times 10^{-15} \text{m}^{-2/3}$, $z = 400\text{m}$, $\sigma_0^2 = 2$.)

intensity of the DPRA is halved and the use of two CCD detectors - instead of a single one - increases the number of noise sources. As for the SPRA-AO module, the probe beam does not have to be split, and only a single detector-noise component is considered. Additionally, the intensity in the Fourier domain is concentrated on the focal domain by the Fourier lens. Compared to the influence of the readout noise on the intensity in the object domain, the effect of noise having the same variance imposed on the Fourier intensity in the back focal plane is lower. This is also the reason that the mode purity associated with SPRA-AO compensation remains almost unchanged. From this perspective, the SPRA-AO system is more robust than the DPRA-AO system.

IV. CONCLUSIONS

In conclusion, we conceived and characterized a low-complexity and high-robustness SPRA-based AO technique capable of compensating for the distortion of the OAM beam in OWC links. Only the intensity of the probe beam in the Fourier domain is required as the measured data of the SPRA wave-front sensor. Moreover, a probe beam expansion scheme was proposed for OAM-OWC links for enhancing the performance of the SPRA. Our simulation results illustrate that the SPRA-AO technique advocated is capable of decontaminating the OAM beam, ameliorating its mode purity and reducing the crosstalk, hence improving the BER performance of OAM-OWC links. Compared to GSA-AO, the SPRA-AO achieves a similar compensation performance at a lower system complexity. Additionally, the results show that the SPRA-AO relying on the proposed expansion scheme accurately improves the mode purity of OAM beams associated with different state indices. Finally, we mathematically analyzed the robustness of the SPRA-AO. Our simulation results show that the background noise degrades the AO compensation performance, regardless whether the SPRA-AO or DPRA-AO approach is used. Under the conditions that both background noise and detector noise are experienced, SPRA-AO exhibits better robustness than DPRA-AO in AO-based OAM-OWC systems.

Our future research may focus on the improvement of the SPRA-AO compensation to make miniaturized low-cost implementations a reality. Moreover, the feasibility of the transmission vector OAM mode will also be explored in our further research. Our work paves the way toward the practical application of PRA-based compensation in the AO field and in OAM-OWC systems.

REFERENCES

- [1] Y. Yang, W. Cheng, W. Zhang, and H. Zhang, "Mode modulation for wireless communications with a twist," *IEEE Transactions on Vehicular Technology*, vol. 67, no. 11, pp. 10 704–10 714, Nov. 2018.
- [2] J. Wang, C. Jiang, K. Zhang, X. Hou, Y. Ren, and Y. Qian, "Distributed Q-learning aided heterogeneous network association for energy-efficient IIoT," *IEEE Transactions on Industrial Informatics*, vol. 16, no. 4, pp. 2756–2764, Nov. 2020.
- [3] Z. Sun, H. Yu, Y. Zhu, and Z. Tian, "An addition-decomposable relaying protocol and signal design for optical wireless communications," *IEEE Transactions on Vehicular Technology*, vol. 67, no. 7, pp. 5980–5993, Feb. 2018.

- [4] H. Yao, T. Mai, J. Wang, Z. Ji, C. Jiang, and Y. Qian, "Resource trading in blockchain-based industrial Internet of Things," *IEEE Transactions on Industrial Informatics*, vol. 15, no. 6, pp. 3602–3609, Jun. 2019.
- [5] J. Wang, C. Jiang, H. Zhang, Y. Ren, K.-C. Chen, and L. Hanzo, "Thirty years of machine learning: The road to Pareto-optimal wireless networks," *IEEE Communications Surveys & Tutorials*, vol. 22, no. 3, pp. 1472–1514, Jan. 2020.
- [6] M. Li, "Orbital angular momentum multiplexing optical wireless communications with adaptive modes adjustment in Internet of Things Network," *IEEE Internet of Things Journal*, vol. 6, no. 4, pp. 6134–6139, Aug. 2019.
- [7] L. Liang, W. Cheng, W. Zhang, and H. Zhang, "Joint OAM multiplexing and OFDM in sparse multipath environments," *IEEE Transactions on Vehicular Technology*, vol. 69, no. 4, pp. 3864–3878, Apr. 2020.
- [8] A. E. Willner, Y. X. Ren, G. D. Xie, Y. Yan, L. Li, Z. Zhao, J. Wang, M. Tur, A. F. Molisch, and S. Ashrafi, "Recent advances in high-capacity free-space optical and radio-frequency communications using orbital angular momentum multiplexing," *Philosophical Transactions*, vol. 375, no. 2087, p. 20150439, Feb. 2017.
- [9] M. I. Dedo, Z. K. Wang, K. Guo, and Z. Y. Guo, "OAM mode recognition based on joint scheme of combining the Gerchberg-Saxton (GS) algorithm and convolutional neural network (CNN)," *Optics Communications*, vol. 456, p. 124696, Feb. 2019.
- [10] W. Zhang, S. Zheng, X. Hui, R. Dong, X. Jin, H. Chi, and X. Zhang, "Mode division multiplexing communication using microwave orbital angular momentum: An experimental study," *IEEE Transactions on Wireless Communications*, vol. 16, no. 2, pp. 1308–1318, Feb. 2017.
- [11] C. H. Kai, Z. K. Feng, M. I. Dedo, P. Huang, K. Guo, F. Shen, J. Gao, and Z. Y. Guo, "The performances of different OAM encoding systems," *Optics Communications*, vol. 430, pp. 151–157, Jan. 2018.
- [12] A. E. Willner, G. D. Xie, L. Li, and Y. X. Ren, "Channel effects and mitigation approaches in free-space and underwater optical communications using orbital angular momentum multiplexing," in *Asia Communications & Photonics Conference*, Wuhan, China, Nov. 2016.
- [13] A. Trichili, K. Park, M. Zghal, B. S. Ooi, and M. Alouini, "Communicating using spatial mode multiplexing: Potentials, Challenges, and Perspectives," *IEEE Communications Surveys Tutorials*, vol. 21, no. 4, pp. 3175–3203, May 2019.
- [14] C. Yang, K. Shan, J. Chen, J. Hou, and S. Chen, "CNN-based phase matching for the OAM mode selection in turbulence heterodyne coherent mitigation links," *IEEE Photonics Journal*, vol. 12, no. 6, pp. 1–13, Dec. 2020.
- [15] G. D. Xie, Y. X. Ren, H. Hao, P. J. Martin, N. Ahmed, Y. Yan, C. J. Bao, L. Li, Z. Zhao, Y. W. Cao, M. Willner, M. Tur, S. J. Dolinar, R. W. Boyd, J. H. Shapiro, and A. E. Willner, "Phase correction for a distorted orbital angular momentum beam using a Zernike polynomials-based stochastic-parallel-gradient-descent algorithm," *Optics Letters*, vol. 40, no. 7, pp. 1197–1200, Apr. 2015.
- [16] A. E. Willner, H. Huang, Y. Yan, Y. X. Ren, and S. Ashraf, "Optical communications using orbital angular momentum beams," *Advances in Optics & Photonics*, vol. 7, no. 1, pp. 66–106, Mar. 2015.
- [17] M. Li, "Phase corrections with adaptive optics and Gerchberg-Saxton iteration: a comparison," *IEEE Access*, vol. 56, no. 2, pp. 284–297, Oct. 2019.
- [18] S. M. Zhao, J. Leach, L. Y. Gong, J. Ding, and B. Y. Zheng, "Aberration corrections for free-space optical communications in atmosphere turbulence using orbital angular momentum states," *Optics Express*, vol. 20, no. 1, pp. 452–461, Jan. 2012.
- [19] Y. X. Ren, H. Huang, J. Y. Yang, Y. Yan, N. Ahmed, Y. Yue, A. E. Willner, K. Birnbaum, J. Choi, B. Erkmen, and S. Dolinar, "Correction of phase distortion of an OAM mode using GS algorithm based phase retrieval," in *Proc. CLEO 2012*, San Jose, California, USA, 2012, p. CF31.4.
- [20] S. Y. Fu, S. K. Zhang, T. L. Wang, and C. Q. Gao, "Pre-turbulence compensation of orbital angular momentum beams based on a probe and the Gerchberg-Saxton algorithm," *Optics Letters*, vol. 41, no. 14, pp. 3185–3188, Jul. 2016.
- [21] H. Chang, X. L. Yin, X. Z. Cui, Z. Z. Zhang, J. X. M. and G. H. Wu, L. J. Zhang, and X. J. Xin, "Adaptive optics compensation of orbital angular momentum beams with a modified Gerchberg-Saxton-based phase retrieval algorithm," *Optics Communications*, vol. 405, no. 2, pp. 271–275, Dec. 2017.
- [22] X. L. Yin, H. Chang, X. Z. Cui, J. X. Ma, Y. J. Wang, G. H. Wu, L. J. Zhang, and X. J. Xin, "Adaptive turbulence compensation with a hybrid input-output algorithm in orbital angular momentum-based free-space optical communication," *Applied Optics*, vol. 57, no. 26, pp. 7644–7650, Sep. 2018.
- [23] J. Fienup, "Comments on "the reconstruction of a multidimensional sequence from the phase or magnitude of its fourier transform";" *IEEE Transactions on Acoustics, Speech, and Signal Processing*, vol. 31, no. 3, pp. 738–739, Jun. 1983.
- [24] J. N. Cederquist, J. R. Fienup, C. C. Wackerman, S. R. Robinson, and D. Kryskowski, "Wave-front phase estimation from Fourier intensity measurements," *Optical Society of America*, vol. 6, no. 7, pp. 1020–1026, Jul. 1989.
- [25] X. Yuan, H. Yao, J. Wang, T. Mai, and M. Guizani, "Artificial intelligence empowered QoS-oriented network association for next-generation mobile networks," *IEEE Transactions on Cognitive Communications and Networking*, pp. 1–1, Mar. 2021.
- [26] H. Yao, B. Zhang, P. Zhang, S. Wu, C. Jiang, and S. Guo, "RDAM: A reinforcement learning based dynamic attribute matrix representation for virtual network embedding," *IEEE Transactions on Emerging Topics in Computing*, vol. 9, no. 2, pp. 901–914, Apr. 2021.
- [27] J. R. Fienup, "Phase retrieval algorithms: a comparison," *Applied Optics*, vol. 21, no. 15, pp. 2758–2769, Aug. 1982.
- [28] S. H. Li, S. Chen, C. Q. Gao, A. E. Willner, and J. Wang, "Atmospheric turbulence compensation in orbital angular momentum communications: Advances and perspectives," *Optics Communications*, vol. 408, pp. 68–81, Feb. 2018.
- [29] X. Zhong, Y. Zhao, G. Ren, S. He, and Z. Wu, "Influence of finite apertures on orthogonality and completeness of Laguerre-Gaussian beams," *IEEE Access*, vol. 6, pp. 8742–8754, Feb. 2018.
- [30] J. A. Anguita, M. A. Neifeld, and B. V. Vasic, "Turbulence-induced channel crosstalk in an orbital angular momentum-multiplexed free-space optical link," *Applied Optics*, vol. 47, no. 13, pp. 2414–2429, May 2008.
- [31] R. L. Phillips and L. C. Andrews, "Spot size and divergence for Laguerre Gaussian beams of any order," *Applied Optics*, vol. 22, no. 5, pp. 643–644, Apr. 1983.
- [32] Y. X. Ren, G. D. Xie, H. Huang, N. Ahmed, Y. Yan, L. Li, C. J. Bao, P. J. Lavery, M. Tur, and M. A. Neifeld, "Adaptive-optics-based simultaneous pre- and post-turbulence compensation of multiple orbital-angular-momentum beams in a bidirectional free-space optical link," *Optica*, vol. 1, no. 6, p. 376, Dec. 2014.
- [33] S. Nyberg, "Optical determination of the correlation coefficient," *Optica Acta: International Journal of Optics*, vol. 19, no. 3, pp. 195–201, 1972.
- [34] J. R. Fienup and T. R. Crimmins, "Reconstruction of the support of an object from the support of its autocorrelation," *Journal of the Optical Society of America*, vol. 72, no. 5, pp. 610–624, Jan. 1982.
- [35] S. Liu, B. M. Hennelly, and J. T. Sheridan, "Digital image watermarking spread space spread spectrum technique based on double random phase encoding," *Optics Communications*, vol. 300, no. 2, pp. 162–177, Jul. 2013.
- [36] B. T. Jiang, Y. H. Qiu, Y. Wen, and Z. Chen, "Modeling and analyzing the noise of CCD," *Electro-Optic Technology Application*, vol. 25, no. 2, pp. 64–67, Apr. 2010.
- [37] H. Faraji and W. J. Maclean, "CCD noise removal in digital images," *IEEE Transactions on Image Processing*, vol. 15, no. 9, pp. 2676–2685, Sep. 2006.
- [38] C. L. Guo, S. Liu, and J. T. Sheridan, "Optical double image encryption employing a pseudo image technique in the Fourier domain," *Optics Communications*, vol. 321, no. 2, pp. 61–72, Jun. 2015.
- [39] G. Healey and R. Kondepudy, "Radiometric CCD camera calibration and noise estimation," *IEEE Transactions on Pattern Analysis and Machine Intelligence*, vol. 16, no. 3, pp. 267–176, Mar. 1994.
- [40] T. Le, R. Chartrand, and T. J. Asaki, "A variational approach to reconstructing images corrupted by Poisson noise," *Journal of Mathematical Imaging and Vision*, vol. 27, no. 3, pp. 257–263, Apr. 2007.
- [41] R. L. Fante, "The effect of source temporal coherence on light scintillations in weak turbulence," *Journal of the Optical Society of America A*, vol. 69, no. 1, pp. 71–73, Jan. 1979.
- [42] S. Y. Fu and C. Q. Gao, "Influences of atmospheric turbulence effects on the orbital angular momentum spectra of vortex beams," *Photonics Research*, vol. 4, no. 5, pp. B1–B4, Oct. 2016.
- [43] X. L. Yin, Y. L. Guo, H. Yan, X. Z. Cui, H. Chang, Q. H. Tian, G. H. Wu, Q. Zhang, B. Liu, and X. J. Xin, "Analysis of orbital angular momentum spectra of Hankel-Bessel beams in channels with oceanic turbulence," *Acta Physica Sinica*, vol. 67, no. 11, p. 114201, Jun. 2018.
- [44] X. Z. Cui, X. L. Yin, H. Chang, Z. C. Zhang, Y. J. Wang, and G. H. Wu, "A new method of calculating the orbital angular momentum spectra of Laguerre-Gaussian beams in channels with atmospheric turbulence," *Chinese Physics B*, vol. 26, no. 11, pp. 232–238, Nov. 2017.



Huan Chang received the Ph.D. degree from the Beijing University of Posts and Telecommunications (BUPT), China, in 2020. She is currently a post-doctor with the School of Information and Electronics, Beijing Institute of Technology. Her main research interests include wireless optical communication and adaptive optics.



Ran Gao received the Ph.D. degree in electronic science and technology from the Beijing Institute of Technology, China, in 2015. He is currently a Professor with the School of Information and Electronics, Beijing Institute of Technology. His research interests include fiber optical sensors, optical waveguide, and measurement instruments.



Xiaoli Yin received the B.E. degree in applied electronic technology, the M.S. degree in optics, and the Ph.D. degree in physical electronics from the Beijing University of Posts and Telecommunications (BUPT), Beijing, China, in 1993, 1996, and 2008, respectively. She is currently a Professor at BUPT. Her research interests include optical communication and signal processing.



Jianping An received the Ph.D. degree from the Beijing Institute of Technology, China, in 1996. He joined the School of Information and Electronics, Beijing Institute of Technology in 1995, where he is currently a Full Professor. He is also the Dean of the School of Information and Electronics, Beijing Institute of Technology. His research interests are in the fields of digital signal processing, cognitive radios, wireless networks, and high-dynamic broadband wireless transmission technology.



Haipeng Yao (M'16, SM'20) is an associate professor in Beijing University of Posts and Telecommunications. Haipeng Yao received his Ph.D. in the Department of Telecommunication Engineering at University of Beijing University of Posts and Telecommunications in 2011. His research interests include future network architecture, network artificial intelligence, networking, space-terrestrial integrated network, network resource allocation and dedicated networks. He has published more than 100 papers in prestigious peer-reviewed journals and

conferences. Dr. Yao has served as an Editor of IEEE Network, IEEE Access, and a Guest Editor of IEEE Open Journal of the Computer Society and Springer Journal of Network and Systems Management. He has also served as a member of the technical program committee as well as the Symposium Chair for a number of international conferences, including IWCMC 2019 Symposium Chair, ACM TUR-C SIGSAC2020 Publication Chair.



Jingjing Wang (S'14-M'19-SM'21) received his B.S. degree in Electronic Information Engineering from Dalian University of Technology, Liaoning, China in 2014 and the Ph.D. degree in Information and Communication Engineering from Tsinghua University, Beijing, China in 2019, both with the highest honors. From 2017 to 2018, he visited the Next Generation Wireless Group chaired by Prof. Lajos Hanzo, University of Southampton, UK. Dr. Wang is currently a postdoc researcher at Department of Electronic Engineering, Tsinghua University.

His research interests include AI enhanced next-generation wireless networks and swarm intelligence. Dr. Wang was a recipient of the Best Journal Paper Award of IEEE ComSoc Technical Committee on Green Communications & Computing in 2018, the Best Paper Award from IEEE ICC and IWCMC in 2019.



Lajos Hanzo (<http://www-mobile.ecs.soton.ac.uk>, https://en.wikipedia.org/wiki/Lajos_Hanzo) (FIEEE'04) received his Master degree and Doctorate in 1976 and 1983, respectively from the Technical University (TU) of Budapest. He was also awarded the Doctor of Sciences (DSc) degree by the University of Southampton (2004) and Honorary Doctorates by the TU of Budapest (2009) and by the University of Edinburgh (2015). He is a Foreign Member of the Hungarian Academy of Sciences and a former Editor-in-Chief of the IEEE

Press. He has served several terms as Governor of both IEEE ComSoc and of VTS. He has published 2000+ contributions at IEEE Xplore, 19 Wiley-IEEE Press books and has helped the fast-track career of 123 PhD students. Over 40 of them are Professors at various stages of their careers in academia and many of them are leading scientists in the wireless industry. He is also a Fellow of the Royal Academy of Engineering (FREng), of the IET and of EURASIP.